13

Electron transport control in quasi-2D-layered ZnO nanoflakes from the standpoint of their effective application in solid-state sensors

© O.E. Glukhova, P.A. Kolesnichenko

Saratov National Research State University,
410012 Saratov, Russia
e-mail: glukhovaoe@info.sgu.ru

Received September 21, 2023
Revised September 21, 2023
Accepted December 21, 2023

The report discusses the electronic characteristics of quasi-2D-layered ZnO nanoflakes, as well as the role of controlling their thickness from the standpoint of increasing the sensitivity of their surface to analytes (acetone, butanol, etc.), which is necessary from the point of view of using these structures as materials for solid gas sensors. The study was conducted using the SCC DFTB method in the DFTB+ software package. ZnO nanoflakes with a hexagonal structure (symmetry group $P63mc$) with a phase surface $(11\bar{2}0)$ were chosen as the object of study. For this object, the optimal width of the 2D-layer was found, after which various analytes were placed on its surface and the resistance was calculated. The result of the study was a diagram of the change in the resistance (conductivity) of zinc oxide when various analytes are on the surface.

Keywords: zinc oxide, analytes, conductivity, quantum transport, SCC DFTB.

DOI: 10.21883/0000000000

Introduction

Zinc oxide is one of the most widely used materials because it is an n-type semiconductor with a valence II−VI with a wide bandgap (~ 3.4,eV [1,2]), high excitation energy and high mobility electrons. It is characterized by chemical stability, ecological compatibility, and low cost of synthesis. Due to its properties, it is used in such important areas of technology as heterogeneous catalysis [3], gas sensors [2,4] and microelectronic devices [5]. This wide range of applications is possible due to the special electronic properties of zinc oxide, manifested by the use of additives or different crystal lattice geometries. In particular, ZnO nanoparticles can be grown in various sizes and with a large number of different shapes, such as fine wires, spheres and spirals [6]. In addition, zinc oxide can also be used in transparent electronics, ultraviolet emitters, piezoelectric devices, optoelectronics, solar cells [7,8]. At the moment, there is no consensus on the toxicity of zinc oxide nanoparticles; perhaps it may be associated with the breakdown of zinc oxide [5,6] into Zn^{2+} ions.

Under standard conditions, ZnO exists in the form of a wurtzite crystal of a hexagonal structure (symmetry group $P63mc$) with four main crystallographic surfaces: non-polar ones $10\bar{1}0$) and ZnO $(11\bar{2}0)$, and polar with the Zn ZnO (0001) face, and also with the O ZnO $000\bar{1}$) face. Non-polar surfaces are of greatest interest, since polar ZnO (0001) and ZnO $(000\bar{1})$ have an uncompensated dipole moment, which apparently prevents the stable formation and existence of these structures [9–13].

The relevance of the topic of scientific work, therefore, lies in the study of ZnO nano-flakes of indicated crystallographic surfaces, because they by themselves are used as detecting elements of multisensory gas sensor systems, the sensitivity of which directly determines the quality of environmental control and human safety.

The purpose of this work is to study the chemoresistive response of S quasi-2D Zinc-oxide nano-flakes to alcohol molecules (acetone, butanol, etc.). To achieve this goal, a technique will be developed for constructing atomistic modelling of supercells of layered quasy 2D-nanoflakes, close to realistic ones based on matching the energy gap value of the band structure of the computer atomistic modeling with the experimentally determined one.

1. Mathematical modeling: approaches and methods

The use of the quantum approach in determining the value S is not implemented in theoretical studies of sensory properties due to the polyatomic nature of supercells and, as a consequence, the complexity and resource-intensiveness of computational procedures. Therefore, the chemoresistive response S was calculated as follows according to the formula (1) [14]:

$$S = \frac{R}{R_0}, \tag{1}$$

where R_0 is resistance of the structure without presence analyte molecules on the surface, R is resistance of the structure with the presence of analyte molecules on its surface.

The resistances required to calculate the response S were calculated using the theory of quantum electron transport using the Landauer-Buttiker formalism and the Keldysh-Green's apparatus for functions [15]. The Landauer-Buttiker

formalism—allows one to calculate the electrical conductivity based on the electron transmission function $T(E)$:

$$G = \frac{2e^2}{h} \int_{-\infty}^{\infty} T(E) F_T(E - E_F) dE, \qquad (2)$$

where e is electron charge, h is Planck's constant, e^2/h is the conductivity quantum, value for a single conductivity channel; this value is doubled to take into account the electron spin, $F_T(E)$ is the thermal broadening function, calculated by the formula:

$$F_T(E) = \frac{1}{4k_B T} \mathrm{sech}\left(\frac{E}{2k_B T}\right), \qquad (3)$$

where k_B is — Boltzmann constant, T is the temperature.

As known, the electron transmission function $T(E)$ characterizes the quantum-mechanical transparency of the conduction channel (a structure segment enclosed between two contacts) depending on the energy of an electron moving in it. The formalism describes the electron transport patterns when only elastic collisions with the crystal lattice atoms are considered during the electron movement via the channel. If we are talking about an 2*D* nanomaterial, as in the case under consideration, then the transmittance function is determined not only by energy, but by two parameters at once, namely, the electron energy and its state, i.e. wave number k of the Brillouin zone. The procedure for calculating the $T(E, k)$ transmittance function is quite resource-intensive, especially in the case of polyatomic super-cells. In this regard, this work presents a new methodology for accelerating the calculation of $T(E)$, based on replacing a three-dimensional crystal with its quasi-2*D*-layered structure with a certain number of layers N, at which an energy characteristic of an 3*D*-crystal is observed, namely the band gap Egap , the value of which is confirmed by experimental data. A similar methodology developed for two-dimensional structures such as graphene and graphane is also presented in the work [16]. The novelty and promise of the methodology lies in the possibility of reduction the true surface profile 2*D*-electron transmittance function $T(E)$, calculated for different energy values E and different states k, based on the results of calculations $T(E, k)$ with a small partition of the first Brillouin zone. Based on the surface profile $T(E, k)$ data, the integral transmittance function $T(E)$, which appears in formula (1), is already calculated. The integral transmittance function T(E) is calculated by averaging over all k.

2. Results

The first step of this work was the construction for models of research targets, namely the structure of the 3*D* ZnO crystal and its quasi-2*D*crystallographic plane ZnO $(11\bar{2}0)$. These models were created in the kview [17] program and are presented in Fig. 1 and 2. Oxygen atoms are marked in red, Zinc atoms are marked in blue.

The next step was to study the electronic structure of these materials. In the software package „DFTB+" their geometric optimization was carried out using the quantum-mechanical density functional method in the tight binding approximation SCC DFTB2 [18]. This method correctly (from a physical point of view) reproduces the electronic properties of nanostructures, the supercells of which contain several hundred and even thousands of atoms [19,20]. In this case, double re-optimization was carried out, implying simultaneous optimization of the atomic structure of the supercell and the periodic box. Thanks to this, the band structure was obtained, on the basis of which Density of States (DOS) graphs were constructed. Based on the obtained graphs, the band gap E_{gap} was calculated, and the Fermi energy was found. Fig. 3 shows the DOS graph for an 3*D* ZnO crystal.

As can be seen from Fig. 3, the band gap calculated *ab initio* is equal to 3.6 eV. The experimentally measured value of E_{gap} for this substance is 3.4 eV [2]. Thus, the error was 6%, so we can say that these results have been successfully tested by experiment.

Similar calculations were performed for the crystallographic surface of ZnO $(11\bar{2}0)$. As mentioned earlier, the basis of the technique is the construction of a quasi-2*D*-model with a band gap similar to the 3*D* crystal. Thus, the structure shown in Fig. 2 was taken as a basis, and then each time its height along the Z axis was increased by one lattice cell (by one layer), after which each time the band structure was calculated, DOS graphs were plotted and the band gap width was calculated. In total, 11 layers of this structure were studied. For comparison, Fig. 4, 5 shows

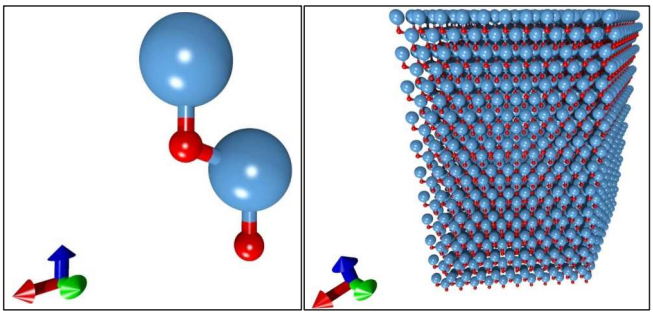

Figure 1. Model of 3*D* ZnO crystal (right) and its lattice cell consisting of four atoms (left).

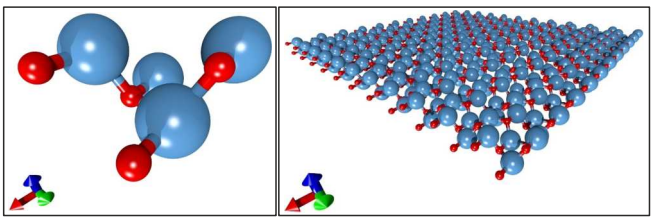

Figure 2. Model of ZnO $(11\bar{2}0)$ in the form of a single-layer 2*D* sheet (right) and its lattice cell consisting of eight atoms (left).

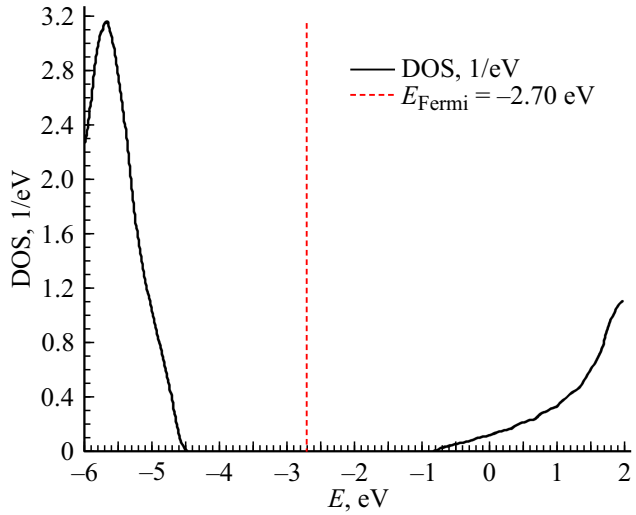

Figure 3. DOS graph for a 3*D* ZnO crystal.

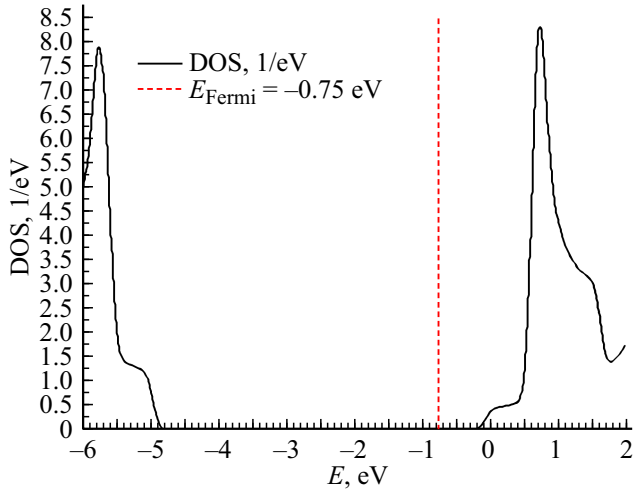

Figure 4. DOS graph for $(11\bar{2}0)$ZnO crystal.

DOS graphs for one layer (shown in Fig. 2) and for four layers of this structure.

As can be seen from Fig. 4, 5, in the case of one layer, the band gap is 4.6 eV, which significantly exceeds the result for the 3*D* crystal. $E_{gap} = 3.6$ eV in the case of four layers. The same kind of result coincides with that in the three-dimensional case.

To summarize, we now show how E_{gap} and E_{Fermi}change when the number of layers of the 2*D*-structure changes. Summary graph of changes in these values depending on the number of layers is presented in Fig. 6.

Based on the presented figure, the following conclusions can be drawn. The band gap decreases from 4.6 to 3.6 eV as the number of layers of the structure increases from 1 to 4, after which it remains unchanged at the level of 3.6 eV. Similarly, the Fermi energy changes significantly in the region from 1 to 4 layers, after which it becomes close to one value of the order of –2.65 eV, practically unchanged from 4 to 11 ZnO layers, $(11\bar{2}0)$.

Based on these results, a structure containing 4 layers was chosen for further work, since this is the minimum number of layers at which a two-dimensional structure has properties similar to the three-dimensional case. Thanks to this choice, further calculations of the transmitance function are carried out in the plane, and not in space, and the number of atoms under study is significantly reduced. This circumstance significantly speeds up and simplifies the calculation.

The next step of the study was the placement of eight different analytes on the surface of four-layer ZnO $(11\bar{2}0)$: acetone, butanol, cyclohexanone, cyclopentanone, ethanol, isopropanol, methanol and octanone. Subsequently, the geometry of such structures was optimized and the optimization energy and charge flow were measured. An example of analyte deposit on the surface of Zinc oxide is shown in Fig. 7.

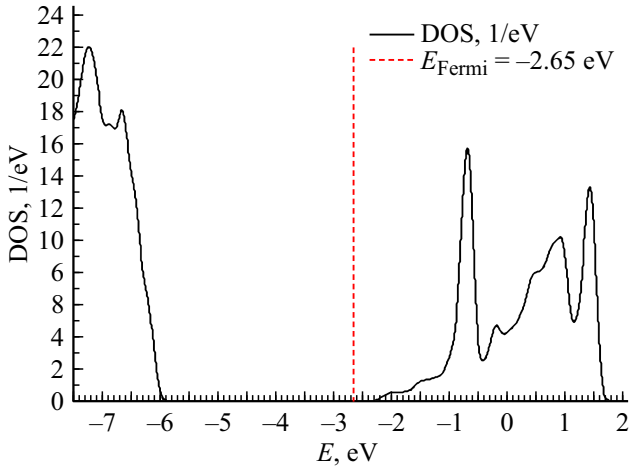

Figure 5. DOS for four layers of ZnO $(11\bar{2}0)$.

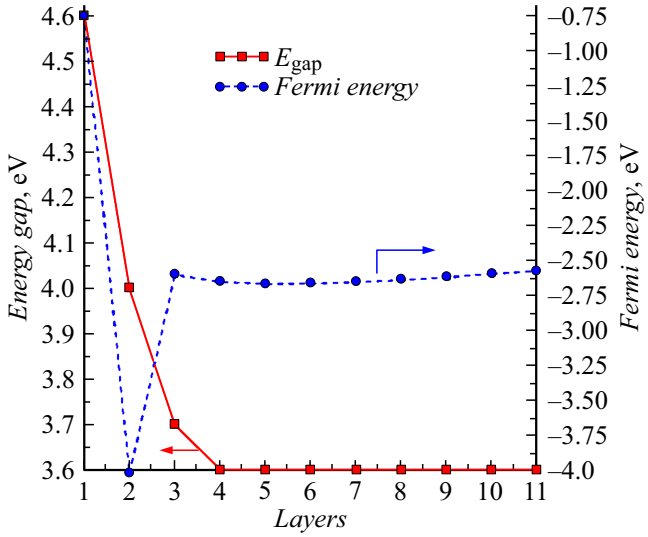

Figure 6. Band gap (solid line) and Fermi energy (dashed line) depending on the number of layers for ZnO $(11\bar{2}0)$.

Table 1. Optimization energy (E)

Analyte	E (analyte), eV	E (ZnO), eV	E (ZnO + analyte), eV	E (bonds), eV	Charge (analyte), e
ACETON	−290.273	−13589.279	−13879.904	−0.352	0.0337
BUTANOL	−376.888		−13967.645	−1.478	0.2113
CYCLOHEXANONE	−470.434		−14060.224	−0.511	0.0386
CYCLOPENTANONE	−403.748		−13994.244	−1.217	0.2239
ETANOL	−243.569		−13834.084	−1.236	0.1915
ISOPROPANOL	−310.333		−13899.977	−0.386	0.0379
METHANOL	−176.815		−13767.308	−1.214	0.1951
OCTANONE	−623.563		−14213.128	−0.286	0.0298

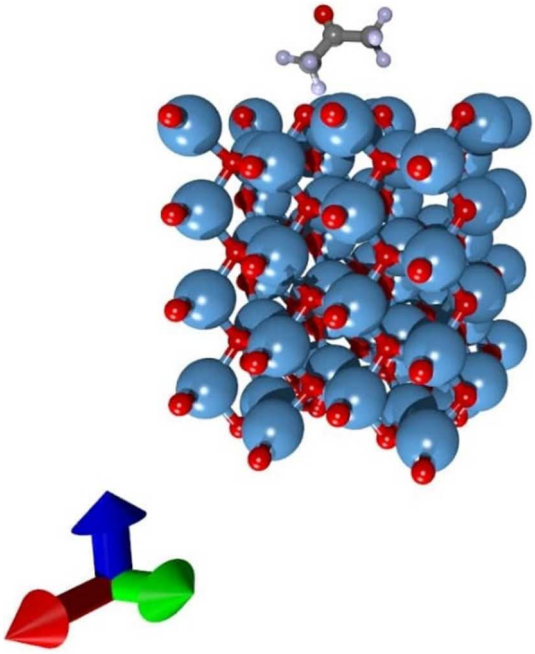

Figure 7. Acetone molecule above the surface of the elementary volume of four-layer zinc oxide.

The results obtained for all studied cases are summarized in a general table 1.

It should also be noted that the table shows the charge on the analyte. From the resulting table it can conclude that all analytes on the surface of zinc oxide form a stable structure (the energy of formation is negative everywhere), the highest (in modulus) energy of formation is for the butanol molecule.

After this, for each case under study, the transmittance function $T(E)$ was calculated using the Landauer-Buttiker theory of quantum electron transport. An example of a graph of the transmittance function (the case without analytes on the surface) is presented in Fig. 8. Then, using formulas (1) and (2), the conductivity (resistance) of the structures under study was calculated. The calculated resistances and chemoresistive response for the case of each of the analytes on the surface, as well as for the case without analytes, are presented in summarized table 2.

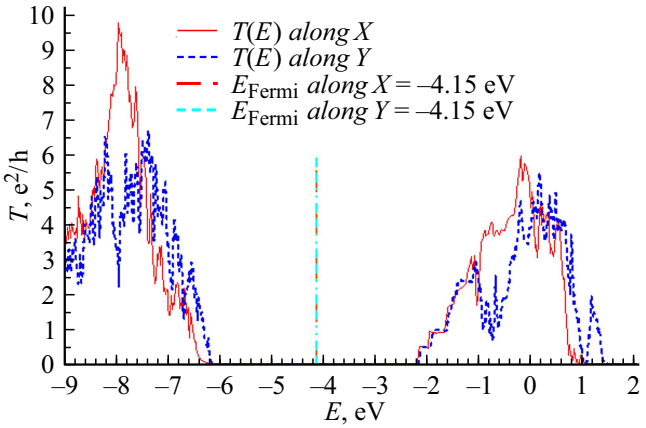

Figure 8. Transmittance function T as a function of energy E with Fermi energy noted for ZnO $(11\bar{2}0)$ without analytes on the surface. The indigo line corresponds to the direction along the X axis, the red line corresponds along the Y axis.

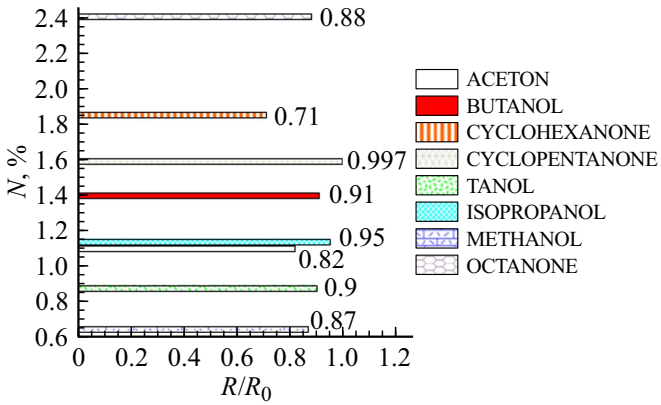

Figure 9. Chemoresistive response for ZnO $(11\bar{2}0)$ with various analytes on the surface along the X-axis.

Table 2. Conductivity ZnO $(11\bar{2}0)$

Analyte	N, %	Along X-axis			Along the Y axis		
		G, fS	R, PΩ	R/R_0	G, fS	R, PΩ	R/R_0
ACETON	1.1	0.361	2.769	0.82	0.109	9.15	0.96
BUTANOL	1.4	0.328	3.052	0.91	0.11	9.076	0.95
CYCLOHEXANONE	1.85	0.419	2.388	0.71	0.121	8.271	0.87
CYCLOPENTANONE	1.59	0.298	3.355	0.997	0.115	8.715	0.92
ETANOL	0.88	0.33	3.032	0.9	0.111	8.978	0.94
ISOPROPANOL	1.14	0.314	3.188	0.95	0.105	9.523	1
METHANOL	0.65	0.34	2.94	0.87	0.112	8.899	0.94
OCTANONE	2.4	0.336	2.974	0.88	0.107	9.303	0.98
Analyte free	–	0.297	3.365	1	0.105	9.509	1

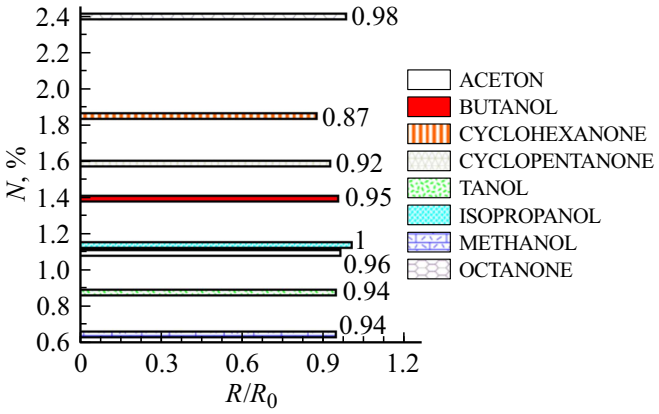

Figure 10. Chemoresistive response for ZnO $(11\bar{2}0)$ with various analytes on the surface along the Y-axis.

In Table 2, the mass fraction of the analyte in the mass of the entire structure is denoted by N, and is calculated as a percentage. The magnitude of the chemo-resistive response S is the ratio of the resistance of the structure to the surface analytes (R) to the resistance of the structure without analytes on surface (R_0).

Based on Table 2, graphs were drawn up of the dependence of the chemo-resistive response for the mass fraction of analytes. The resulting graphs are presented in Fig. 9 — with the direction of electron transport along the X axis, and in Fig. 10 with the direction along the Y axis.

From the obtained graphs it is clear that in both cases the resistance became lower when analytes were deposited. However, the results turned out to be different for different directions of electron transport. This circumstance is likely due to the asymmetry of the location of the analytes on the surface of Zinc oxide relative to the X and Y axes.

Conclusion

The propose of the work was to construct an effective practices for creating realistic atomistic modeling of a substance exemplified by zinc oxide, followed by testing with experimental data, as well as to study the chemiresistive response as a characteristic that determines the sensitivity of ZnO nanoflakes to analytes.

To do this, the following series of actions were performed. First, in the software package „Kvazar“ the structures of zinc oxide under consideration as well as its crystallographic surface $(11\bar{2}0)$ were modeled. Then, for the $3D$ crystal, geometry optimization was carried out in the DFTB+ software package, the electronic structure was determined using the SCC DFTB method, and the DOS graph was plotted. From this graph, the band gap was determined to be 3.6 eV. The obtained result turned out to differ from the experimentally measured one by 6%, which proves the validity of the *ab initio* calculation method. After that, the densities of states were similarly calculated for ZnO $(11\bar{2}0)$ with the number of supercells in height from 1 to 11. It was determined that four layers of this quasi-$2D$ structure are sufficient for its electronic characteristics (Fermi energy, band gap) to correspond to those of a bulk crystal. Then eight different analytes were placed on the selected structure, after which characteristics such as bond energy and flow of charge were calculated in a similar way. Next, using the Landauer-Buttiker theory of quantum transport, the transmittance function of the structures was calculated, on the basis of which the linear resistance (resistance per unit length) and, finally, the chemoresistive response for each of the studied analytes were calculated

As a result of the work, DOS graphs were obtained for the previously mentioned structures with Fermi energies marked on them. Based on these results, a graph was drawn

up of the dependence of these values on the number of layers. In addition, the transmittance function versus energy was plotted, as well as the chemo-resistive response was plotted for the studied analytes along two different electron transport directions was plotted.

The following conclusions may be drawn from the obtained results.

Four layers of a quasi-2*D* of the ZnO sheet are sufficient for its properties to correspond to a bulk crystal. This circumstance greatly simplifies further calculations of the transmittance function, since instead of a three-dimensional case, a two-dimensional one is considered.

Another important conclusion can be drawn based on the obtained chemo-resistive response graphs. It can be noted that the appearance of alcohols on the surface of Zinc oxide entails a decrease in its resistance, i.e. the conductivity of the entire structure increases. In addition, it can be noted that the indicated characteristics differ for different directions of electronic transport. This can be explained by the asymmetry of the position of the analyte molecules above the surface of Zinc oxide.

The developed new methodology for constructing realistic models can significantly facilitate and speed up the calculations of various electronic parameters of the structures under study. The new knowledge regarding the interaction of Zinc oxide with analytes can help in a deeper understanding of the processes underlying the operation of gas sensors, the main material of which is zinc oxide nano-flakes, which will create the basis for the development of more advanced methods for the production and quality control of these devices, and this, in turn, directly affects the quality of human life, since it allows more precise control of the presence of pollutants in the air.

Conflict of interest

The authors declare that they have no conflict of interest.

References

[1] M. Hellström, K. Jorner, M. Bryngelsson, S.E. Huber, J. Kullgren, T. Frauenheim, P. Broqvist. J. Phys. Chem. C, **117**, 17004 (2013). DOI: 10.1021/jp404095x
[2] H. Morko**,** Ü. Özgür. *Zinc Oxide: Fundamentals, Materials, and Device Technology* (Wiley-VCH Verlag GmbH & Co. KGaA, Weinheim, 2009), DOI: 10.1002/9783527623945
[3] C. Ratnasamy, J. Wagner. Catalys. Rev., **51**, 325 (2009). DOI: 10.1080/01614940903048661
[4] Z.L. Wang. J. Phys. Condensed Matter, **16**, 829 (2004). DOI: 10.1088/0953-8984/16/25/R01
[5] K. Schilling, B. Bradford, D. Castelli, E. Dufour, J.F. Nash, W. Pape, S. Schulte, I. Tooley, J. Van den Bosch, F. Schellauf. Photochem. Photobiolog. Sci., **9**, 495 (2010). DOI: 10.1039/b9pp00180h
[6] T. Xia, M. Kovochich, M. Liong, L. Mädler, B. Gilbert, H. Shi, J.I. Yeh, J.I. Zink, A.E. Nel. ACS Nano, **2**, 2121 (2008). DOI: 10.1021/nn800511k
[7] K. Nomura, H. Ohta, K. Ueda, T. Kamiya, M. Hirano, H. Hosono. Science, **300** (5623), 1269 (2003). DOI: 10.1126/science.1083212
[8] T. Nakada, Y. Hirabayashi, T. Tokado, D. Ohmori, T. Mise. Solar Energy, **77** (6), 739 (2004). DOI: 10.1016/j.solener.2004.08.010
[9] C. Zhou, J. Kang. J. Mater. Sci.: Mater. Electron., **19**, 229 (2008). DOI: 10.1007/s10854-007-9561-5
[10] S.H. Overbury, P.V. Radulovic, S. Thevuthasan, G.S. Herman, M.A. Henderson, C.H.F. Peden. Surf. Sci., **410**, 106 (1998). DOI: 10.1016/S0039-6028(98)00307-0
[11] C.B. Duke, A.R. Lubinsky. Surf. Sci., 50, 605 (1975). DOI: 10.1016/0039-6028(75)90049-7
[12] M. Sambi, G. Granozzi, G.A. Rizzi, M. Casarin, E. Tondello. Surf. Sci., **319**, 149 (1994). DOI: 10.1016/0039-6028(94)90577-0
[13] M. Galeotti, A. Atrei, U. Bardi, G. Rovida, M. Torrini, E. Zanazzi, A. Santucci, A. Klimov. Chem. Phys. Lett., **222**, 349 (1994). DOI: 10.1016/0009-2614(94)87073-X
[14] N.K. Plugotarenko, T.N. Myasoedova, S.P. Novikov, T.S. Mikhailova. Chemosensors, **10** (4), 126 (2022). DOI: 10.3390/chemosensors10040126
[15] S. Datta. *Electronic Transport in Mesoscopic Systems* (Cambridge University Press, Cambridge, 1995). DOI: 10.1017/CBO9780511805776
[16] O.E. Glukhova, D.S. Shmygin. Beilstein J. Nanotechnol., **9**, 1254 (2018). DOI: 10.3762/bjnano.9.117
[17] O.E. Glukhova, G.V. Savostyanov, M.M. Slepchenkov. Proced. Mater. Sci., **6**, 256 (2014). DOI: 10.1016/j.mspro.2014.07.032
[18] M. Elstner, D. Porezag, G. Jungnickel, J. Elsner, M. Haugk, Th. Frauenheim, S. Suhai, G. Seifert. Phys. Rev. B, **58**, 7260 (1998). DOI: 10.1103/PhysRevB.58.7260
[19] O.E. Glukhova, M.M. Slepchenkov. J. Phys. Chem. C, **120**, 17753 (2016). DOI: 10.1021/acs.jpcc.6b05058
[20] M.M. Slepchenkov, D.S. Shmygin, G. Zhang, O.E. Glukhova. Nanoscale, **11**, 16414 (2019). DOI: 10.1039/C9NR05185F

Translated by V.Prokhorov